The role of bottom currents on the morphological development around a drowned carbonate platform, NW South China Sea

Yu Kaiqi[1, 2, 3], Alves Tiago M.[4], Li Wei[1, 2, 3], Li Shuang[1, 2, 3], Li Jian[1, 2, 3], Zhao Fang[1, 2, 3], Wu Shiguo[3, 5], Zhan Wenhuan[1, 2, 3]

1) CAS Key Laboratory of Ocean and Marginal Sea Geology, South China Sea Institute of Oceanology, Chinese Academy of Sciences, Guangzhou 510301, China

2) Southern Marine Science and Engineering Guangdong Laboratory (Guangzhou), Guangzhou 511458, China

3) University of Chinese Academy of Sciences, Beijing 100049, China

4) 3D Seismic Laboratory, School of Earth and Environmental Sciences, Cardiff University, Cardiff CF10 3AT, United Kingdom

5) Institute of Deep-Sea Science and Engineering, Chinese Academy of Sciences, Sanya 572000, China

Abstract: The seafloor around carbonate platforms is largely shaped and modified by downslope processes. However, the role of alongslope processes, including bottom currents, on the morphological development of carbonate platforms remains poorly understood. Here, we use high-resolution multibeam bathymetric data and two-dimensional seismic profiles to investigate the detailed sea-floor morphology around the Zhongjianbei carbonate platform (ZCP) in the northwest South China Sea. A series of depositional bodies and erosional channels are identified to the south of the ZCP and are interpreted as contourite drifts and channels resulted from the interaction between bottom currents and bathymetric features. In addition, active fluid seepages have led to the formation of widespread pockmarks on the seafloor. Importantly, the contourite channels and widespread pockmarks also show a close

relationship in their distribution. We propose that the contourite channels around the ZCP are evolved from the coalescence of pockmarks under the persistent erosion of bottom currents. Based on the morphological analysis, we reconstruct the past bottom-current pathways around the ZCP that are parallel to the platform slopes and heading to the south. This study provides new insights into the formation of complex bathymetry and helps understanding how bottom currents and active fluid seepages can influence the morphological development around carbonate platforms.

Keywords: carbonate platform; seafloor morphology; contourite channels; bottom currents; fluid seepages; South China Sea.

1. Introduction

Carbonate platforms are formed in the photic zone and occur widely on continental margins and abyssal plains of tropical seas (Betzler et al., 1995; Wilson et al., 1998; Eberli et al., 2010; Mulder et al., 2012; Lüdmann et al., 2013; Shao et al., 2017; Betzler and Eberli, 2019). They form important carbonate factories in source-to-sink systems, and thus feed abundant sediments to surrounding sedimentary basins (Merino-Tomé et al., 2012; Counts et al., 2018; Michel et al., 2019). In addition, the development of carbonate platforms significantly changes the surrounding seafloor morphology, and thereby influences the regional sedimentary and oceanographic dynamics (Mulder et al., 2017; Wunsch et al., 2017; Nolting et al., 2018; Principaud et al., 2018).

Due to their importance in oceanography, sedimentology and submarine geohazards, the morphological development of carbonate platforms has drawn increasing attention in recent years (Menier et al., 2014; Purkis et al., 2014; Prat et al., 2016). Studies have shown that

downslope and along-slope processes are two of the most important mechanisms shaping the seafloor around carbonate platforms (Mulder et al., 2012; Principaud et al., 2017; Eberli et al., 2019). Downslope processes include submarine mass wasting, slope failure and turbidity currents, which form particular seafloor bedforms such as sediment waves, slide scars, creep, submarine channels and gullies (Dowdeswell et al., 2006; Heinio and Davies, 2009; Li et al., 2016, 2018). Bathymetric features formed by downslope processes have been investigated in many regions such as the Mozambique Channel (Courgeon et al., 2016; Counts et al., 2018), Australian North West Shelf (Rankey, 2017; Rinke-Hardekopf et al., 2018) and Little and Great Bahama Bank (Mulder et al., 2017). Together with downslope processes, along-slope bottom currents can also significantly shape and modify the seafloor morphology, producing erosional and depositional bedforms (García et al., 2009; Stow et al., 2009; Rebesco et al., 2014; Miramontes et al., 2019a). In recent years, an increasing number of articles has documented the importance of bottom currents on the flanks of carbonate platforms in the Maldives (Lüdmann et al., 2013), Bahamian archipelago (Mulder et al., 2019) and South China Sea (Shao et al., 2017). They have proved that bottom currents redistribute sediments shed by the carbonate platforms and erode their flanks to generate sediment drifts, moats, contourite channels and furrows. However, compared to the downslope processes around carbonate platforms, the importance of alongslope currents in such platforms is still poorly understood.

Due to the favorable latitude, oceanographic and tectonic setting of the northwest South China Sea, a large number of carbonate platforms have developed in this region since the early Miocene (Wu et al., 2014, 2016; Gao et al., 2019). The bathymetry of the northwest South China Sea has largely influenced the oceanographic setting in this region, especially the pathways of bottom currents (Chen et al., 2016; Yin et al., 2021). This study focuses on investigating the role of bottom currents on the morphological development around an

isolated, drowned carbonate platform, the Zhongjianbei carbonate platform (ZCP). High-resolution multibeam bathymetric data and two-dimensional (2D) seismic lines are used to: 1) characterize the bathymetry around the ZCP and evidence for the presence of bottom-current activity; 2) reconstruct past bottom-current pathways around the ZCP; and 3) propose a representative model explaining the complex seafloor bedforms observed around the ZCP and other carbonate platforms.

2. Regional Setting

2.1 Geological Background

The South China Sea is the largest (3.5×106 km2) and deepest (> 5000 m) marginal sea in the western Pacific Ocean (Wang and Wang, 1990). The northwest South China Sea was formed after the late Cretaceous by distinct tectonic activities: continental rifting, continental breakup, and post-rift tectonism (Zhou et al., 1995; Li et al., 2015a; Lei et al., 2020; Zhang et al., 2021). It comprises several Cenozoic rift basins such as the Pearl River Mouth, Qiongdongnan, Yinggehai and Zhongjiannan Basins (Zhao et al., 2020). In the Paleocene, hyperextension led to the formation of a regional basement high in the northwest South China Sea, later developing as a shallow platform on which the Xisha Islands developed (Tapponnier et al., 1990; Li et al., 2015a). The northwest South China Sea entered a phase of thermal subsidence in the early Miocene (Wu et al., 2009), with post-rift tectonics promoting the growth of carbonate platforms (Wu et al., 2014; Zhu et al., 2017).

Carbonate platforms in the northwest South China Sea mainly occur above the Xisha and Guangle highs, and are separated into two distinct groups by the Zhongjian canyon (Lu et al., 2018; Gao et al., 2019). The Zhongjianbei carbonate platform (ZCP), the focus of this study,

is an isolated and drowned carbonate platform located to the north-east of the Guangle high and southwest of the Zhongjian canyon, at a water depth between 350 and 1200 m (Figs.1, 2 and 3). The Neogene and Quaternary stratigraphy in the surrounding region of the ZCP is divided into five formations: the Ledong, Yinggehai, Huangliu, Meishan, and Sanya formations (Gao et al., 2019). Based on regional correlations with adjacent basins (Li et al., 2015b; Lu et al., 2018; Gao et al., 2019), four seismic horizons, T30, T40, T50 and T60, have been identified in the seismic profiles, corresponding to the bottom interfaces of Pliocene, late Miocene, middle Miocene and early Miocene strata, respectively (Figs.1C, 4 – 6).

2.2 Oceanography

The South China Sea is a semi-enclosed marginal sea connected to the Pacific Ocean via the Luzon Strait (Liu et al., 2008). Four major water masses are identified: surface, intermediate, deep and bottom water (Tian et al., 2006; Quan et al., 2016; Yin et al., 2021). Surface water moves cyclonically between 0 and 750 m at a speed of up to 100 cm s−1, whereas the South China Sea intermediate water circulates anticyclonically between 750 and 1500 m water depth at a speed of 5 – 15 cm s−1 (Quan et al., 2016). Deep water flows at a depth of 1500 to 2200 m, while bottom water occurs below 2200 m. Both deep and bottom waters have an average speed lower than 5 cm s−1 (Zeng et al., 2016; Zhu et al., 2019).

The South China Sea was isolated from the North Pacific subtropical gyre in the late Miocene due to the formation of the Luzon Strait (Tian et al., 2006). This event resulted in a major palaeo-oceanographic shift, which promoted the anti-clockwise flow of surface water masses in the Northwest South China Sea (Yin et al., 2021). Present day surface water circulation is dominated by a Western Boundary Current flowing southward (Fig.1B). Flowing through the study area all year, this current can reach a depth of about 600 m, a maximum instantaneous

velocity of more than 1 cm s−1 and play a key role in the distribution of mass, energy and heat in the South China Sea (Quan et al., 2016). High-resolution ocean circulation models for the western Pacific and northern Indian Oceans record a predominant anti-clockwise circulation for intermediate water masses of the South China Sea (Liang et al., 2019).

3. Data and Methods

This study is based on the interpretation of high-resolution multibeam bathymetric data and two-dimensional (2D) multi-channel seismic reflection profiles. The multibeam bathymetric data were acquired by a SeaBeam 2112 system in 2008. The horizontal and vertical resolution of the bathymetric data are 100 m (cell size) and 3 m (3‰ of the water depth). The bathymetric data were imported and analyzed in Global Mapper® to investigate the bathymetry around the ZCP in detail.

The two-dimensional (2D) seismic reflection data were acquired by the China National Petroleum Company (CNPC) in 2005 and processed by using the software package Pro-Max from Landmark®. Seismic data were migrated with a common midpoint (CMP) spacing of 12.5 m, and a main frequency bandwidth of 30 Hz to 45 Hz, for a main frequency of 35 Hz. Vertical resolution for these seismic data approaches 25 m. The 2D seismic reflection data were interpreted by using Landmark®.

The multibeam bathymetric data in this study covers more than 3000 km2 (Figs.1, 2 and 3). We have specifically investigated the dimension, incision depth, and scale of seafloor features formed around the ZCP. Moreover, based on the 2D seismic profiles crossing erosional features in the study area, we were able to investigate subsurface structures and their relationship with seafloor features (Figs.3 – 5). Changes in seismic attributes (e.g.,

amplitude, polarity, uniformity and continuity) were used to interpret faults, palaeo-pockmark, palaeo-channel and fluid-escape structures.

4. Results

Based on the analysis of multibeam bathymetric data and two-dimensional seismic profiles, we have identified several seafloor morphological features and subsurface structures.

4.1 Seafloor morphology

The ZCP has a flat top and three flanking slopes facing the northeast, southeast and southwest (Fig.1B). On its southern flanks, the seafloor predominantly comprises alongslope morphological features such as channels and elongated depressions (Figs.2 and 3). Alongslope morphological features are absent on the northeast flank of the ZCP; they are replaced by base-of-slope sediments (Fig.1B).

4.1.1 Seafloor erosional features

Erosional features are the most remarkable and dominant alongslope morphological features on the southern flanks of the ZCP (Figs.2 and 3). They are parallel and oriented in a similar direction to the slopes bordering the ZCP. They show a relatively constant spacing of about 1.5 km and occur in combination with elongated and mounded depositional bodies (Figs.2 and 3). Topographic profiles crossing these erosional features show a similar ‘U-shaped’ geometry (Figs.2D, 2E, 3C and 3D). Their width ranges from 0.5 to 2 km, and their maximum depth of incision is 160 m. The length of these erosional features decreases to the south, with maximum and minimum lengths of 20 km and 7 km, respectively. Two channel-

like erosional features occur on the bottom of southwest and south-east slopes of the ZCP, presenting smoother thalwegs and shallower incision depths than other channel-like erosional features in the study area (Figs.2 and 3).

4.1.2 Seafloor depressions

A large number of depressions are identified on the southern flanks of the ZCP, close to the previous erosional features (Figs.2 and 3). These depressions are crescent, elongated and circular in plan-view. They are 50- to 100-m deep with a diameter ranging from hundreds of meters to more than 1 km. Some of these isolated depressions are observed at the ends of channel-like erosional features (e.g., C1 and C2; Fig.2C). In addition, several elongated depressions forming distinct trails are also extended in the direction of channel-like erosional features (e.g., C3 and C7; Figs.2C and 3B). The elongated depressions, when distributed in trails, have a similar morphology to the channel-like erosional features, especially when their width and incision depth are considered (Figs.2 and 3). Furthermore, the relics of elongated depressions exist at the bases of channel-like erosional features (e.g., C6 and C7; Fig.3B).

4.2 Subsurface Structures

Mounded depositional bodies, palaeo-depressions, palaeo-erosional features, pipe and chimney structures, mainly occur in strata younger than Horizon T50 (15.5 Myr). They mainly occur to the south of the ZCP (Figs.4 – 6).

4.2.1 Mounded depositional bodies

Mounded depositional bodies are observed above Horizon T30 (5.5 Myr) on the southern flanks of the ZCP (Figs.4 and 5). The width of these depositional bodies ranges from 2 to 3 km and their thickness reaches more than 300 m (Figs.4 and 5). They are characterised by continuous, parallel and convex internal seismic reflections with low to medium amplitude. The mounds are truncated by erosional features and pinch out towards the ZCP (Figs.4A, 4B, 5A and 5D).

4.2.2 Palaeo-depressions and paleo-erosional features

Multiple palaeo-depressions and palaeo-erosional features have been identified in strata above Horizon T40 (10.5 Myr) (Figs.4 – 6). The lower boundaries of them are continuous and concave seismic reflections with high amplitude, and some of them coincide with Horizon T30 (5.5 Myr) (Figs.5B and 5C). Palaeo-depressions are filled with parallel, continuous strata. Chaotic strata occur at their bases (Figs.5A and 5B).

Similar to the palaeo-depressions described above, other palaeo-erosional features are imaged as concave seismic reflections with medium to high amplitude that truncate the surrounding strata (Figs.4 – 6). Palaeo-erosional features usually show a 'U-shaped' geometry in cross-section and correlate well with other channel-like erosional features on the seafloor (Figs.5D and 5E). Palaeo-erosional features clearly migrate laterally, as shown by the vertical superposition of multiple palaeo-erosional features (Figs.5C, 5D and 5E).

4.2.3 Fluid pipes and chimneys

Fluid pipe and chimney structures are observed on the south flanks of the ZCP, but are rarely identified on the north flank of the ZCP (Figs.4 – 6). They form cones or pipes in seismic

images, and their internal seismic reflections are chaotic with low to medium amplitude (Figs.4C, 4D, 5B, 5C and 5E). These structures, rooted in strata below Horizons T30 or T40, develop vertically into younger strata (Figs.4 and 5). Some end at the bases of the palaeo-depressions or palaeo-erosional features, while other are linked with surface depressions (Figs.4B and 5A).

5. Discussion

5.1 Evidence for the occurrence of bottom currents

A series of channel-like erosional features and elongated depositional bodies are identified on the southern flanks of the ZCP. Generally, these erosional features and depositional bodies are distributed in an alongslope direction, indicating a common formation mechanism.

Channel-like erosional features to the south of the ZCP have the following morphological characteristics (Figs.2 and 3): 1) they are parallel to the regional contours and the strikes of platform slopes; 2) they present 'U-shaped' geometries in cross-section, with the average width of 1.5 km and the incision depth of 120 m; 3) they reveal a constant spacing of 1.2 km. Based on these observations, downslope processes (e.g., mass wasting or turbidity currents) can be excluded as the origin for these channels. We propose that these channel-like erosional features comprise contourite channels, similar to the features documented in the western Mediterranean (de Weger et al., 2020), Gulf of Cadiz (García et al., 2009) and western South China Sea (Yin et al., 2021).

Depositional bodies along the flanks of the ZCP are characterised by their variable mounded geometries, especially their distinctly elongated and mounded shape (Figs.2 and 3). Their

internal seismic reflections are smooth, parallel and continuous, often interbedded with transparent zones (Figs.4 and 5). Internal seismic reflections thin out towards the platform flanks and are truncated by erosional channels away from the ZCP. They are also separated from the platform by an alongslope erosional channel (Figs.4 and 5).

Our interpretation provides the robust evidence for discrete contourite drifts along the flanks of the ZCP, which were accumulated by the persistent action of bottom currents. The two channels that are closest to the southern flanks of the ZCP, separate the contourite drifts from the carbonate platform, and are therefore considered as erosional moats (Figs.2 – 5). Similar contourite drifts, combined with erosional moats formed by alongslope processes, are documented in regions such as the Danish Basin (Surlyk and Lykke-Andersen, 2007), Western Mediterranean Sea (Miramontes et al., 2019a), Bahamian Archipelago (Mulder et al., 2019), SE Brazil (Alves, 2010) and Great Australian Bight (Jackson et al., 2019). Furthermore, palaeo-depressions and associated palaeo-erosional features identified in the seismic profiles may be the residue of palaeo-pockmarks and palaeo-channels, suggesting the important activity of bottom currents in the past (Yin et al., 2021).

5.2 Reconstructing the pathways of bottom currents around the ZCP

Previous studies have used multiple methods to reconstruct the pathways of bottom-currents, including: a) numerical simulations (Chen et al., 2016; Miramontes et al., 2019a), b) palaeo-bathymetric analyses (de Weger et al., 2020) and, c) in situ current measurements via moorings and landers (Miramontes et al., 2019b). In addition, the concept of space-for-time substitution – referring to the understanding of long-term landform development by comparing similar landforms of different ages or at different stages of evolution – has been previously used to reconstruct the evolution of submarine channels (Micallef et al., 2014). In

particular, the direction and relative velocity of bottom currents can be inferred from the trend, depth and asymmetry of contourite channels (García et al., 2009; Stow et al., 2009).

Here, we utilize the concept of space-for-time substitution to investigate the development of contourite channels around the ZCP, and thereby reconstruct the pathways of palaeo-bottom currents. Seafloor pockmarks occur in trails that co-exist with the contourite channels observed around the ZCP (Figs.2 and 3). Kilhams et al. (2011) have demonstrated that trails of pockmarks can coalesce to form furrows, or immature channels under the continuous erosion of bottom currents. We therefore propose that the contourite channels around the ZCP are also developed from pockmark trails (Figs.2 and 3); they are interpreted as leading to the inception of contourite channels. Under the erosion of bottom currents, some of the pockmarks coalesced to form immature channels, which are characterized by rugged thalwegs (e.g., channels C3, C6 and C7; Figs.2 and 3). Immature channels subsequently evolved into mature channels under the further erosion of bottom currents. We also propose that the direction of a contourite channel indicates both the original strike of pockmarks in a trail and the flow direction of bottom currents. This is the reason why the contourite channels along the flanks of the ZCP developed towards the southeast and southwest, respectively (Fig.7). Bottom-current should flow to the direction which these contourite channels developed towards, from north of the ZCP to the south (Fig.7). Seafloor bathymetry also greatly impact the hydrodynamics of bottom currents (Hernández-Molina et al., 2006; de Castro et al., 2020): The ZCP splits the bottom currents into two branches and intensified the erosion to the slop close to the base, generating contourite channels along the southeast and southwest flanks of the ZCP (Fig.7).

Palaeo-erosional features indicate that palaeo-channels were formed in upper Miocene strata (Figs.4 – 6). However, on the northeast flank of the ZCP, the palaeo-bottom currents gradually diminished in strength after the Late Miocene and left no erosional features on the

modern sea-floor (Fig.6). The identification of palaeo-pockmarks and palaeo-channels on the seismic profiles indicates that bot tom currents were already active in the late Miocene (5.5 Myr), reshaping pre-existing pockmarks and contributing to the formation of palaeo-channels (Figs.4 and 5). Unfortunately, due to the lack of three-dimensional seismic data, it is impossible to characterise the overall morphology of palaeo-pockmarks and paleo-channels, particularly when the time-dependent morphological evolution of palaeo-pockmarks towards contourite channels is considered. Based on the interpretated seismic data, we propose that the change from pockmarks to contourite channels occurred after the late Miocene (5.5 Myr), as pockmarks and contourite channels on the modern seafloor reveal such change – from pockmarks to channels – is ongoing (Figs.2, 3 and 7).

5.3 Interaction between bottom currents and fluid seepages

The morphology around carbonate platforms can be significantly shaped and modified by alongslope processes (bottom currents) via the formation of moats, contourite channels and drifts (Lüdmann et al., 2013; Betzler and Eberli, 2019; Eberli et al., 2019; Mulder et al., 2019). However, the complex morphology around the ZCP is marked by large numbers of parallel contourite channels, which occur in combination with widespread pockmarks (Figs.2 and 3), a pattern rarely observed in other parts of the world.

Based on the interpretation of high-resolution seismic reflection data, Gao et al. (2019) demonstrated that late Cenozoic magmatism led to the formation of hydrothermal systems and the build-up of local overpressures, both responsible for active fluid seepages around the Xisha Islands. Fluid escape structures are widely identified on the seismic profiles on the flanks of the ZCP (Figs.4 and 5). Around the ZCP, fluid escape structures rooted in middle to upper Miocene strata have been identified beneath the interpreted channels and pockmarks

(Figs.4 and 5). These structures, imaged in seismic data as columnar features with dimmed internal reflections due to local amplitude and velocity anomalies, mark the pathways for focused fluid venting that generated seafloor pockmarks (Pilcher and Argent, 2007; León et al., 2010; Cartwright and Santamarina, 2015; Bertoni et al., 2017; Velayatham et al., 2018). The local seafloor relief produced by the pockmarks led to the enhancement of bottom-current erosion in their leeward and/or windward side and, as a result, pockmarks become elongated along the flowing direction of bottom currents (Andresen et al., 2008; Kilhams et al., 2011).

The initiation of fluid seepages and bottom currents, generating fluid escape structures and palaeo-channels respectively, are documented by the seismic profiles acquired around the ZCP (Figs.4 – 6). Fluid seepages mainly occurred on the southeast and southwest flanks of the ZCP at different times. On the southwest flank, fluid escape structures are rooted in strata older than horizon T30, hence indicating a maximum age of 5.5 Myr (Fig.4). However, on the southeast flank the fluid escape structures occur below horizon T30 – though lining to the palaeo-channels and pockmarks buried by the sedimentary stratum younger than T30. This reveals an onset for pockmarks before 5.5 Myr (Fig.5). In general, present or palaeo morphologies, including pockmarks and channels, show a close relationship with fluid escape structures formed by the active fluid seepages. Therefore, the active fluid seepages generated pockmarks around the ZCP, and the interaction between bottom currents and fluid seepages led to the maintenance and channelization of these same pockmarks.

In summary, we propose that the special and complex morphology around the ZCP results from the interaction between bottom currents and fluid seepages on the seafloor (Fig.8). The erosional force of bottom currents was enhanced by active fluid seepages when the bottom currents flowed across pre-existing or developing pockmarks.

6. Conclusions

This study shows that the seafloor morphology around the ZCP was reshaped by the interaction between bottom currents and active fluid seepages. Based on the analysis of high-resolution bathymetric data and two-dimensional (2D) seismic-reflection data, in this work we reached the following conclusions:

1) A series of alongslope morphological features, such as moats, contourite channels and drift, have been identified on the seafloor and in some older strata around the ZCP. These features corroborate the importance of bottom current activities around the ZCP. Moreover, a large number of pockmarks are identified in the study area, and show a close relationship with overlying contourite channels.

2) Based on the concept of space-for-time substitution, we suggest that the contourite channels around the ZCP are formed through the coalescence of isolated pockmarks under the action of bottom currents. The evolution of contourite channels around the ZCP includes three distinct stages: mature channels (C1, C2, C4 and C5), immature channels (C3, C6 and C7) and pockmark trails.

3) Based on the evolution stages of the contourite channels and their spatial relationship with seafloor pockmarks, the channels are inferred to develop from north to south. Hence, the bottom currents around the ZCP are speculated to flow from the north of the ZCP to the south.

4) Active fluid seepages led to the widespread distribution of pockmarks around the ZCP, and these pre-existed (or developing) pockmarks have significantly contributed to the formation of contourite channels. The complex bathymetry around ZCP is, therefore, a result of the interaction between bottom currents and seafloor fluid seepages.

Fig.8 Three-dimensional conceptual model revealing that bottom current erosion is not the unique factor leading to the complex seafloor bedforms around the ZCP. Active fluid seepages induced by post-rift magmatism led to the widespread fluid escape structures and pockmarks in the surroundings of ZCP (Gao et al., 2019). The pre-existence of the pockmarks around ZCP are indispensable requirements for the formation of contourite channels under the erosion of bottom currents. Therefore, the interaction between bottom currents and active fluid seepages generated the complex bathymetry in the study area, which comprises moats, contourite channels, contourite drift and pockmarks. The yellow arrows are proposed pathways for bottom currents in the surroundings of ZCP, and blue arrows indicate the gravity flows in the Zhongjian canyon. The multibeam bathymetric data are from Lu et al. (2018).

Acknowledgements

We thank the PetroChina Hangzhou Research Institute of Geology for the permissions to release the seismic data. This study was financially supported by the Key Special Project for Introduced Talents Team of Southern Marine Science and Engineering Guangdong Laboratory (Guangzhou) (No. GML2019ZD0104), the Guangdong Basic and Applied Basic Research Foundation (No. 2020B1515020016), the National Natural Science Foundation of Guangdong Province (No. 2020A1515010497), the National Natural Science Foundation of China (No. 41876054) and the Guangdong Pearl River Talents Program (No. 2017GC01 0510). Dr. Wei Li is specially funded by the CAS Pioneer Hundred Talents Program (Y8SL011001). The two anonymous reviewers are thanked for their review and constructive comments.

References

Alves, T. M., 2010. A 3-D morphometric analysis of erosional features in a contourite drift from offshore SE Brazil. Geophysical Journal International, 183: 1151-1164.

Andresen, K. J., Huuse, M., and Clausen, O. R., 2008. Morphology and distribution of Oligocene and Miocene pockmarks in the Danish North Sea – Implications for bottom current activity and fluid migration. Basin Research, 20: 445-466.

Bertoni, C., Kirkham, C., Cartwright, J., Hodgson, N., and Rodriguez, K., 2017. Seismic indicators of focused fluid flow and cross-evaporitic seepages in the eastern Mediterranean. Marine and Petroleum Geology, 88: 472-488.

Betzler, C., and Eberli, G. P., 2019. Miocene start of modern carbonate platforms. Geology, 47: 771-775.

Betzler, C., Brachert, T. C., and Kroon, D., 1995. Role of climate in partial drowning of the Queensland Plateau carbonate platform (northeastern Australia). Marine Geology, 123: 11-32.

Cartwright, J., and Santamarina, C., 2015. Seismic characteristics of fluid escape pipes in sedimentary basins: Implications for pipe genesis. Marine and Petroleum Geology, 65: 126-140.

Chen, H., Xie, X., Zhang, W., Shu, Y., Wang, D., Vandorpe, T., et al., 2016. Deep-water sedimentary systems and their relationship with bottom currents at the intersection of Xisha Trough and northwest sub-basin, South China Sea. Marine Geology, 378: 101-113.

401 Counts, J. W., Jorry, S. J., Leroux, E., Miramontes, E., and Jouet, G., 2018. Sedimentation
402 adjacent to atolls and volcano-cored carbonate platforms in the Mozambique Channel (SW
403 Indian Ocean). Marine Geology, 404: 41-59.

404 Courgeon, S., Jorry, S. J., Camoin, G. F., BouDagher-Fadel, M. K., Jouet, G., Révillon, S., et
405 al., 2016. Growth and demise of Cenozoic isolated carbonate platforms: New insights from
406 the Mozambique Channel seamounts (SW Indian Ocean). Marine Geology, 380: 90-105.

407 de Castro, S., Hernández-Molina, F. J., Rodríguez-Tovar, F. J., Llave, E., Ng, Z. L., Nishida,
408 N., et al., 2020. Contourites and bottom current reworked sands: Bed facies model and
409 implications. Marine Geology, 428: 106267.

410 de Weger, W., Hernández-Molina, F. J., Flecker, R., Sierro, F. J., Chiarella, D., Krijgsman,
411 W., et al., 2020. Late Miocene contourite channel system reveals intermittent overflow
412 behavior. Geology, 48: 1194-1199.

413 Dowdeswell, J. A., Evans, J., Cofaigh, C. Ó., and Anderson, J. B., 2006. Morphology and
414 sedimentary processes on the continental slope off Pine Island Bay, Amundsen Sea, West
415 Antarctica. Geological Society of America Bulletin, 118: 606-619.

416 Eberli, G. P., Anselmetti, F. S., Isern, A. R., and Delius, H., 2010. Timing of changes in sea-
417 level and currents along Miocene platforms on the Marion Plateau, Australia, Cenozoic
418 carbonate systems of Australasia. SEPM Society for Sedimentary Geology Special
419 Publication, 95: 219-242.

420 Eberli, G. P., Betzler, C., and Frank, T., 2019. Characteristics of modern carbonate contourite
421 drifts. Sedimentology, 66: 1163- 1191.

Gao, J., Bangs, N., Wu, S., Cai, G., Han, S., Ma, B., et al., 2019. Post-seafloor spreading magmatism and associated magmatic hydrothermal systems in the Xisha uplift region, northwestern South China Sea. Basin Research, 31: 688-708.

García, M., Hernández-Molina, F. J., Llave, E., Stow, D. A. V., León, R., Fernández-Puga, M. C., et al., 2009. Contourite erosive features caused by the Mediterranean outflow water in the Gulf of Cadiz: Quaternary tectonic and oceanographic implications. Marine Geology, 257: 24-40.

Heinio, P., and Davies, R. J., 2009. Trails of depressions and sediment waves along submarine channels on the continental margin of Espirito Santo Basin, Brazil. Geological Society of America Bulletin, 121: 698-711.

Hernández-Molina, F., Larter, R., Rebesco, M., and Maldonado, A., 2006. Miocene reversal of bottom water flow along the Pacific margin of the Antarctic Peninsula: Stratigraphic evidence from a contourite sedimentary tail. Marine Geology, 228: 93-116.

Jackson, C. A. L., Magee, C., and Hunt-Stewart, E. R., 2019. Cenozoic contourites in the eastern Great Australian Bight, offshore southern Australia: Implications for the onset of the Leeuwin Current. Journal of Sedimentary Research, 89: 199-206.

Kilhams, B., McArthur, A., Huuse, M., Ita, E., and Hartley, A., 2011. Enigmatic large-scale furrows of Miocene to Pliocene age from the central North Sea: Current-scoured pockmarks? Geo-Marine Letters, 31: 437-449.

Lei, C., Alves, T. M., Ren, J., and Tong, C., 2020. Rift structure and sediment infill of hyperextended continental crust: Insights from 3D seismic and well data (Xisha Trough, South China Sea). Journal of Geophysical Research: Solid Earth, 125 (5): e2019JB018610.

León, R., Somoza, L., Medialdea, T., Hernández-Molina, F. J., Vázquez, J. T., Díaz-del-Rio, V., et al., 2010. Pockmarks, collapses and blind valleys in the Gulf of Cádiz. Geo-Marine Letters, 30: 231-247.

Li, C. F., Li, J., Ding, W., Franke, D., Yao, Y., Shi, H., et al., 2015a. Seismic stratigraphy of the central South China Sea Basin and implications for neotectonics. Journal of Geophysical Research: Solid Earth, 120: 1377-1399.

Li, W., Alves, T. M., Wu, S., Rebesco, M., Zhao, F., Mi, L., et al., 2016. A giant, submarine creep zone as a precursor of large-scale slope instability offshore the Dongsha Islands (South China Sea). Earth and Planetary Science Letters, 451: 272-284.

Li, W., Alves, T. M., Wu, S., Völker, D., Zhao, F., Mi, L., et al., 2015b. Recurrent slope failure and submarine channel incision as key factors controlling reservoir potential in the South China Sea (Qiongdongnan Basin, South Hainan Island). Marine and Petroleum Geology, 64: 17-30.

Li, W., Krastel, S., Alves, T. M., Urlaub, M., Mehringer, L., Schürer, A., et al., 2018. The Agadir slide offshore NW Africa: Morphology, emplacement dynamics, and potential contribution to the Moroccan Turbidite System. Earth and Planetary Science Letters, 498: 436-449.

Liang, L., Xue, H., and Shu, Y., 2019. The Indonesian Through-flow and the circulation in the Banda Sea: A modeling study. Journal of Geophysical Research: Oceans, 124: 3089-3106.

Liu, Q., Kaneko, A., and Sun, J. L., 2008. Recent progress in studies of the South China Sea circulation. Journal of Oceanography, 64: 753-762.

Lu, Y., Li, W., Wu, S., Cronin, B. T., Lyu, F., Wang, B., et al., 2018. Morphology, architecture, and evolutionary processes of the Zhongjian canyon between two carbonate platforms, South China Sea. Interpretation, 6: SO1-SO15.

Lüdmann, T., Kalvelage, C., Betzler, C., Fürstenau, J., and Hübscher, C., 2013. The Maldives, a giant isolated carbonate platform dominated by bottom currents. Marine and Petroleum Geology, 43: 326-340.

Menier, D., Pierson, B., Chalabi, A., Ting, K. K., and Pubellier, M., 2014. Morphological indicators of structural control, relative sea-level fluctuations and platform drowning on present-day and Miocene carbonate platforms. Marine and Petroleum Geology, 58: 776-788.

Merino-Tomé, Ó., Porta, G. D., Kenter, J. A. M., Verwer, K., Harris, P. M., Adams, E. W., et al., 2012. Sequence development in an isolated carbonate platform (lower Jurassic, Djebel Bou Dahar, High Atlas, Morocco): Influence of tectonics, eustacy and carbonate production. Sedimentology, 59: 118-155.

Micallef, A., Ribó, M., Canals, M., Puig, P., Lastras, G., and Tubau, X., 2014. Space-for-time substitution and the evolution of a submarine canyon-channel system in a passive progradational margin. Geomorphology, 221: 34-50.

Michel, J., Laugié, M., Pohl, A., Lanteaume, C., Masse, J. P., Donnadieu, Y., et al., 2019. Marine carbonate factories: A global model of carbonate platform distribution. International Journal of Earth Sciences, 108: 1773-1792.

Miramontes, E., Garreau, P., Caillaud, M., Jouet, G., Pellen, R., Hernández-Molina, F. J., et al., 2019a. Contourite distribution and bottom currents in the NW Mediterranean Sea: Coupling seafloor geomorphology and hydrodynamic modelling. Geomorphology, 333: 43-60.

Miramontes, E., Penven, P., Fierens, R., Droz, L., Toucanne, S., Jorry, S. J., et al., 2019b. The influence of bottom currents on the Zambezi Valley morphology (Mozambique Channel, SW Indian Ocean): In situ current observations and hydrodynamic modelling. Marine Geology, 410: 42-55.

Mulder, T., Ducassou, E., Eberli, G. P., Hanquiez, V., Gonthier, E., Kindler, P., et al., 2012. New insights into the morphology and sedimentary processes along the western slope of Great Bahama Bank. Geology, 40: 603-606.

Mulder, T., Ducassou, E., Hanquiez, V., Principaud, M., Fauquembergue, K., Tournadour, E., et al., 2019. Contour current imprints and contourite drifts in the Bahamian Archipelago. Sedimentology, 66: 1192-1221.

Mulder, T., Gillet, H., Hanquiez, V., Ducassou, E., Fauquembergue, K., Principaud, M., et al., 2017. Carbonate slope morphology revealing a giant submarine canyon (little Bahama Bank, Bahamas). Geology, 46: 31-34.

Nolting, A., Zahm, C. K., Kerans, C., and Nikolinakou, M. A., 2018. Effect of carbonate platform morphology on syndepositional deformation: Insights from numerical modeling. Journal of Structural Geology, 115: 91-102.

Pilcher, R., and Argent, J., 2007. Mega-pockmarks and linear pockmark trains on the West African continental margin. Marine Geology, 244: 15-32.

Prat, S., Jorry, S. J., Jouet, G., Camoin, G., Vella, C., Le Roy, P., et al., 2016. Geomorphology and sedimentology of a modern isolated carbonate platform: The Glorieuses Archipelago, SW Indian Ocean. Marine Geology, 380: 272-283.

Principaud, M., Mulder, T., Hanquiez, V., Ducassou, E., Eberli, G. P., Chabaud, L., et al., 2018. Recent morphology and sedimentary processes along the western slope of Great Bahama Bank (Bahamas). Sedimentology, 65: 2088-2116.

Principaud, M., Ponte, J. P., Mulder, T., Gillet, H., Robin, C., and Borgomano, J., 2017. Slope-to-basin stratigraphic evolution of the northwestern Great Bahama Bank (Bahamas) during the Neogene to Quaternary: Interactions between downslope and bottom currents deposits. Basin Research, 29: 699-724.

Purkis, S., Kerr, J., Dempsey, A., Calhoun, A., Metsamaa, L., Riegl, B., et al., 2014. Large-scale carbonate platform development of Cay Sal Bank, Bahamas, and implications for associated reef geomorphology. Geomorphology, 222: 25-38.

Quan, Q., Xue, H., Qin, H., Zeng, X., and Peng, S., 2016. Features and variability of the South China Sea western boundary current from 1992 to 2011. Ocean Dynamics, 66: 795-810.

Rankey, E. C., 2017. Seismic architecture and seismic geomorphology of heterozoan carbonates: Eocene – Oligocene, browse basin, northwest shelf, Australia. Marine and Petroleum Geology, 82: 424-443.

Rebesco, M., Hernández-Molina, F. J., Van Rooij, D., and Wåhlin, A., 2014. Contourites and associated sediments controlled by deep-water circulation processes: State-of-the-art and future considerations. Marine Geology, 352: 111-154.

Rinke-Hardekopf, L., Reuning, L., Bourget, J., and Back, S., 2018. Syn-sedimentary deformation as a mechanism for the initiation of submarine gullies on a carbonate platform to slope transition, Browse Basin, Australian North West Shelf. Marine and Petroleum Geology, 91: 622-630.

Shao, L., Li, Q., Zhu, W., Zhang, D., Qiao, P., Liu, X., et al., 2017. Neogene carbonate platform development in the NW South China Sea: Litho-, bio- and chemo-stratigraphic evidence. Marine Geology, 385: 233-243.

Stow, D. A. V., Hernández-Molina, F. J., Llave, E., Sayago-Gil, M., Díaz del Río, V., and Branson, A., 2009. Bedform-velocity matrix: The estimation of bottom current velocity from bedform observations. Geology, 37: 327-330.

Surlyk, F., and Lykke-Andersen, H., 2007. Contourite drifts, moats and channels in the upper Cretaceous chalk of the Danish Basin. Sedimentology, 54: 405-422.

Tapponnier, P., Lacassin, R., Leloup, P. H., Schärer, U., Dalai, Z., Haiwei, W., et al., 1990. The Ailao Shan/Red River metamorphic belt: Tertiary left-lateral shear between Indochina and South China. Nature, 343: 431-437.

Tian, J., Yang, Q., Liang, X., Xie, L., Hu, D., Wang, F., et al., 2006. Observation of Luzon Strait transport. Geophysical Research Letters, 33: L19607.

Velayatham, T., Holford, S. P., and Bunch, M. A., 2018. Ancient fluid flow recorded by remarkably long, buried pockmark trains observed in 3D seismic data, Exmouth Plateau, northern Carnarvon Basin. Marine and Petroleum Geology, 95: 303-313.

Wang, D., Wu, S., Qin, Z., Spence, G., and Lü, F., 2013. Seismic characteristics of the Huaguang mass transport deposits in the Qiongdongnan Basin, South China Sea: Implications for regional tectonic activity. Marine Geology, 346: 165-182.

Wang, L., and Wang, P., 1990. Late Quaternary paleoceanography of the South China Sea: Glacial-interglacial contrasts in an enclosed basin. Paleoceanography, 5: 77-90.

554 Wilson, P. A., Jenkyns, H. C., Elderfield, H., and Larson, R. L., 1998. The paradox of
555 drowned carbonate platforms and the origin of Cretaceous Pacific guyots. Nature, 392: 889-
556 894.

557 Wu, S., Yang, Z., Wang, D., Lü, F., Lüdmann, T., Fulthorpe, C., et al., 2014. Architecture,
558 development and geological control of the Xisha carbonate platforms, northwestern South
559 China Sea. Marine Geology, 350: 71-83.

560 Wu, S., Yuan, S., Zhang, G., Ma, Y., Mi, L., and Xu, N., 2009. Seismic characteristics of a
561 reef carbonate reservoir and implications for hydrocarbon exploration in deepwater of the
562 Qiongdongnan Basin, northern South China Sea. Marine and Petroleum Geology, 26: 817-
563 823.

564 Wu, S., Zhang, X., Yang, Z., Wu, T., Gao, J., and Wang, D., 2016. Spatial and temporal
565 evolution of Cenozoic carbonate platforms on the continental margins of the South China
566 Sea: Response to opening of the ocean basin. Interpretation, 4: SP1-SP19.

567 Wunsch, M., Betzler, C., Lindhorst, S., Lüdmann, T., Eberli, G. P., and Della Porta, G., 2017.
568 Sedimentary dynamics along carbonate slopes (Bahamas archipelago). Sedimentology, 64:
569 631- 657.

570 Yin, S., Hernandez-Molina, F. J., Lin, L., Chen, J., Ding, W., and Li, J., 2021. Isolation of the
571 South China Sea from the North Pacific Subtropical Gyre since the latest Miocene due to
572 formation of the Luzon Strait. Scientific Report, 11: 1562.

573 Zeng, L., Wang, D., Chen, J., Wang, W., and Chen, R., 2016. SCSPOD14, a South China Sea
574 physical oceanographic dataset derived from in situ measurements during 1919 – 2014.
575 Scientific Data, 3: 160029.

576 Zhang, C., Sun, Z., Manatschal, G., Pang, X., Qiu, N., Su, M., et al., 2021. Syn-rift magmatic
577 characteristics and evolution at a sediment-rich margin: Insights from high-resolution seismic
578 data from the South China Sea. Gondwana Research, 91: 81-96.

579 Zhao, F., Alves, T. M., Xia, S., Li, W., Wang, L., Mi, L., et al., 2020. Along-strike
580 segmentation of the South China Sea margin imposed by inherited pre-rift basement
581 structures. Earth and Planetary Science Letters, 530: 115862.

582 Zhou, D., Ru, K., and Chen, H. Z., 1995. Kinematics of Cenozoic extension on the South
583 China Sea continental margin and its implications for the tectonic evolution of the region.
584 Tectonophysics, 251: 161-177.

585 Zhu, W., Xie, X., Wang, Z., Zhang, D., Zhang, C., Cao, L., et al., 2017. New insights on the
586 origin of the basement of the Xisha uplift, South China Sea. Science China (Earth Sciences),
587 60: 2214-2222.

588 Zhu, Y., Sun, J., Wang, Y., Li, S., Xu, T., Wei, Z., et al., 2019. Overview of the multi-layer
589 circulation in the South China Sea. Progress in Oceanography, 175: 171-182.

590

591

Figures

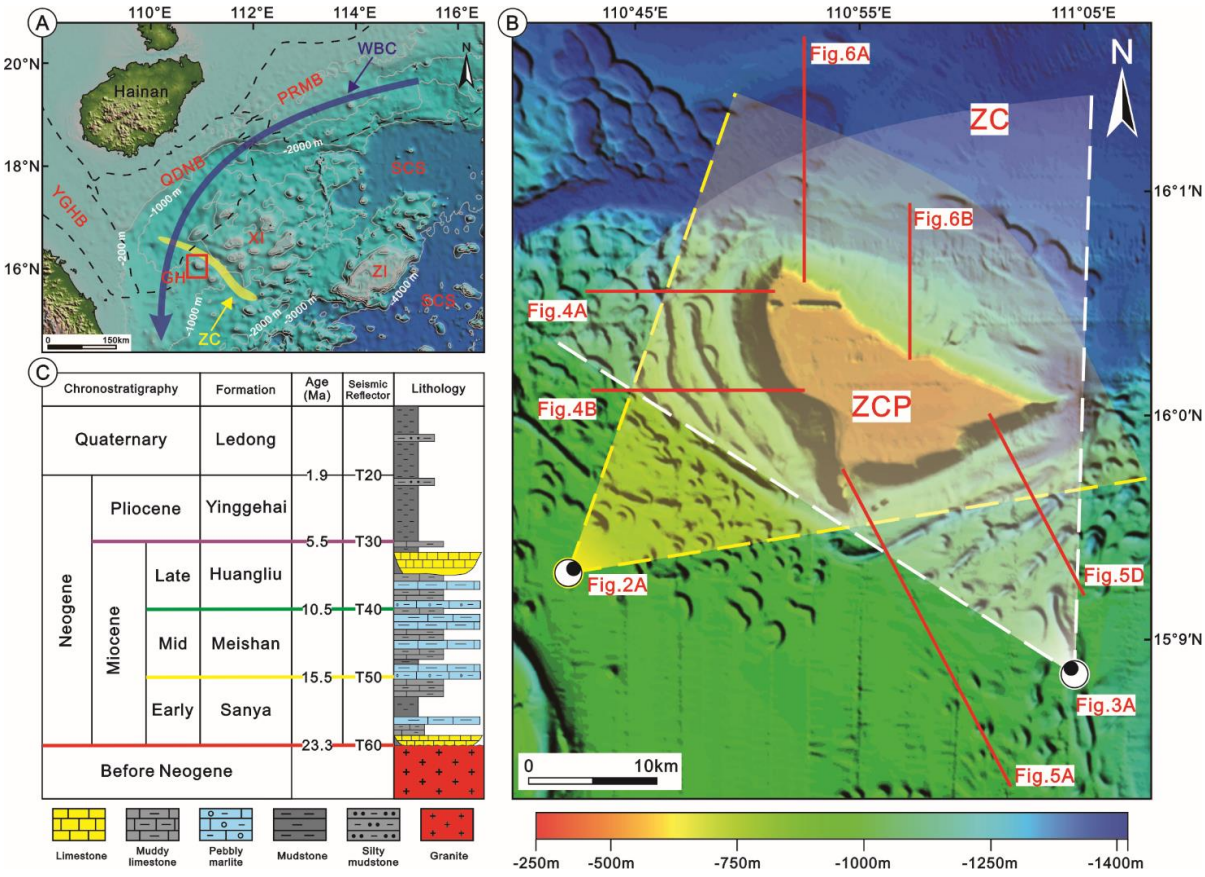

Fig.1 A) Regional geological setting of the study area. Modified from Gao *et al*. (2019). Black dashed lines indicate the boundaries of sedimentary basins in the Northwest South China Sea. The dark blue curve arrow indicates the Western Boundary Currents (WBC) of South China Sea, and the yellow belt shows the layout of Zhongjian canyon (ZC). The red box indicates the location of study area shown as Fig.1B. B) Multibeam bathymetric map of the study area (modified after Lu *et al.* (2018)). The Zhongjianbei carbonate platform (ZCP) is located at the very center of the study area, next to the Zhongjian canyon (ZC) in the northeast. Red solid lines indicate the locations of two-dimensional seismic profiles acquired in the vicinity of the ZCP, and the 'eye' symbols combined with yellow and white dashed lines indicate the viewpoints of Fig.2A and Fig.3A respectively. C) Stratigraphic column of the study area based on Lu *et al*. (2018) and Gao *et al*. (2019). Key: YGH, Yinggehai Basin; QDNB, Qiongdongnan Basin; PRMB, Pearl River Mouth Basin; XI, Xisha Islands; ZI, Zhongsha Islands; GH, Guangle high; SCS, South China Sea.

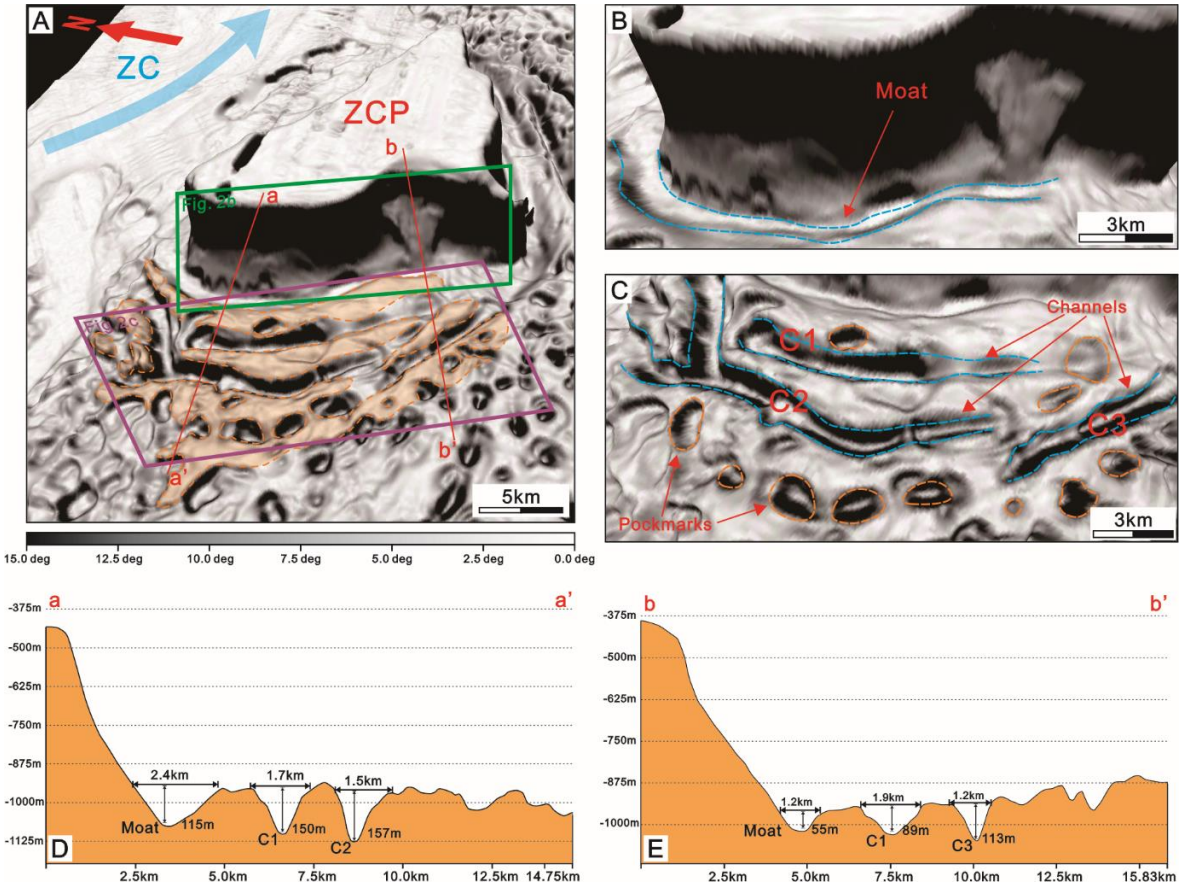

608

609 Fig.2 A) Three-dimensional slope gradient map depicting a southwest view of the ZCP with
610 the viewpoint shown in Fig.1B. Blue solid arrow indicates the direction of gravity flows in
611 the ZC. Orange dashed lines highlight the features associated with alongslope currents. Red
612 solid lines indicate the locations of bathymetric profiles (shown in Figs.2D and 2E) across the
613 platform slope and associated channel-like erosional features. The multibeam bathymetric
614 data for morphological description is from Lu et al. (2018). B) Moat along the flanks of the
615 ZCP. C) Details of three channels (C1, C2 and C3) formed in the southwest flanks of ZCP,
616 which are sub-parallel to the moat. Numerous pockmarks are observed around these channels.
617 D) and E) Bathymetric profiles revealing the cross-section geometries (width and depth of
618 incision) of the moat and channels.

619

620 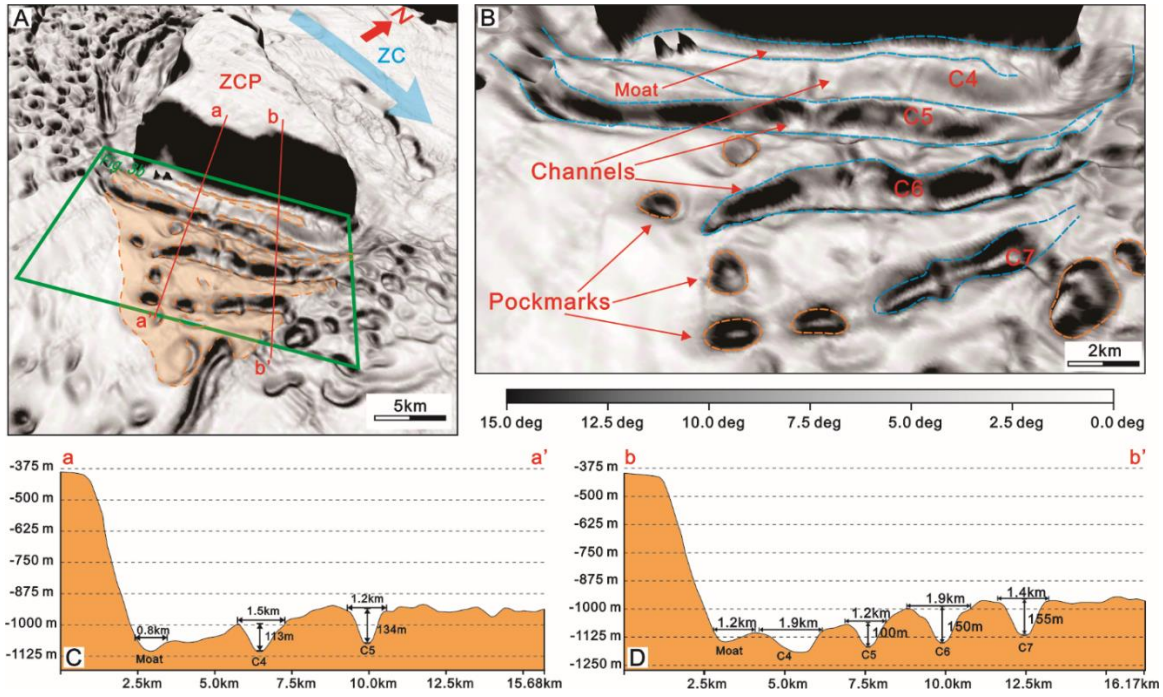

621 Fig.3 A) Slope gradient map revealing the three-dimensional morphology of the southeast
622 flank of the ZCP. The features associated with alongslope processes are indicated by orange
623 dashed lines. In the ZC, gravity flows to the southeast direction are indicated by the blue
624 arrow. Red solid lines show the distribution of the bathymetric profiles crossing the platform
625 flanks, moat and channels. The viewpoint of Fig.3A is shown in Fig.1B. B) Four channels
626 (C4, C5, C6 and C7) are identified in the southeast flank of the ZCP. They are sub-parallel to
627 the observed moat and surrounded by pockmarks. C) and D) Bathymetric profiles (a – a' and
628 b – b' in Fig.3A) showing the U-shaped cross-sections, width and incision depth of moat and
629 channels. The bathymetry is after Lu et al. (2018).

630

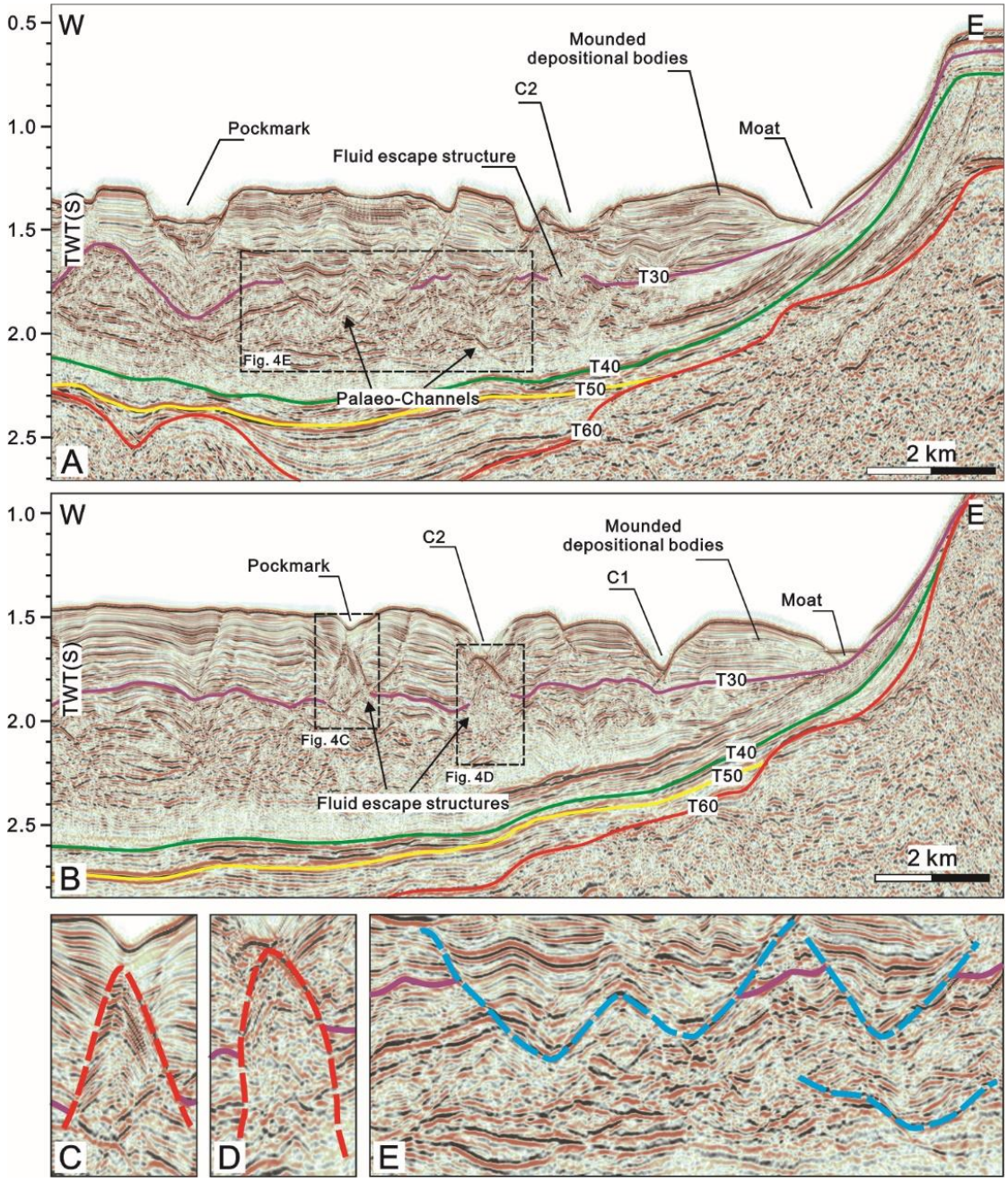

631

632 Fig.4 A) and B) Seismic profiles imaging the sub-seafloor strata in the southwest flank of the
633 ZCP and associated erosional and depositional features. Stratigraphic horizons T60, T50, T40
634 and T30 and sub-surface structures are also illustrated. The locations of the seismic profiles
635 are shown in Fig.1B. The seismic data is after Wang et al. (2013) and Wu et al. (2014). C)
636 and D) Zoomed-in seismic profile showing the fluid escape structures (depicted by red
637 dashed lines) cross Horizon T30 (shown as purple solid line) and their link with the
638 depressions on the seafloor. E) Zoomed-in seismic section revealing the presence of palaeo-
639 channels (shown as blue dashed lines), which truncate or underlie the Horizon T30 (purple
640 solid lines).

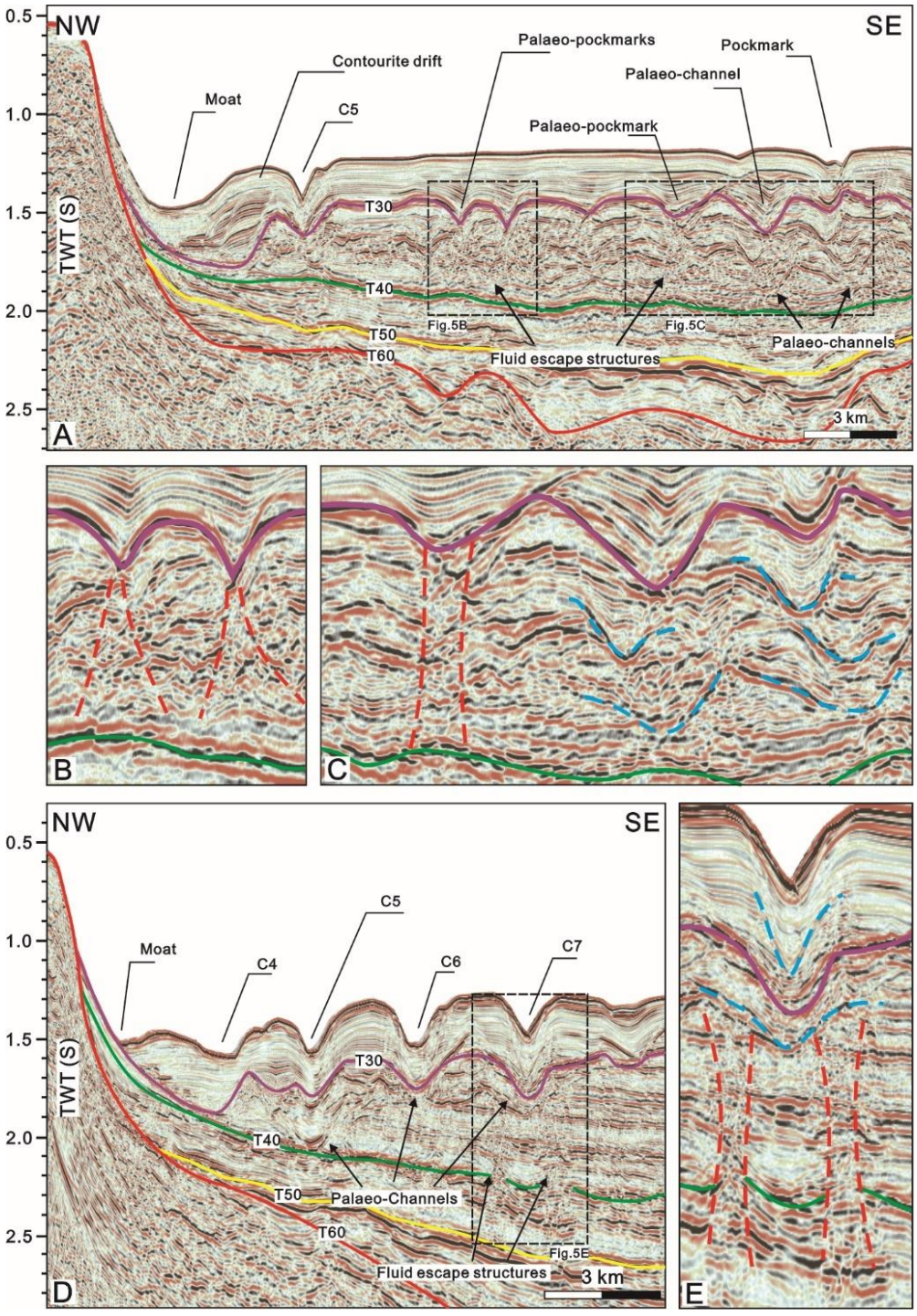

Fig.5 A) Seismic profile highlighting the multiple seafloor features and structures in the southeast flank of the ZCP (see location in Fig.1B). Moats, channels, pockmarks and contourite drifts are identified on the seafloor. Palaeo-channel, palaeo- pockmarks and fluid escape structures are observed in older strata. B) Zoomed-in seismic profile showing the relationship between fluid escape structures (outlined by red dashed lines) and palaeo-

pockmarks. Purple and green solid lines represent seismic reflection T30 and T40, respectively. C) Zoomed-in seismic profile revealing that the migration of palaeo-channels (shown as blue dashed lines) and palaeo-pockmarks is associated with fluid escape features (depicted as red dashed lines). D) Seismic profile showing subsurface structures and the seafloor bathymetry, including moat and channels (C4, C5, C6 and C7) on the southeast flank of the ZCP. E) Zoomed-in seismic profile revealing the spatial relationship between modern channels, palaeo-channels (shown as blue dashed lines), fluid escape features (outlined by red dashed lines) and Horizon T40 (shown as green solid lines). The original seismic profiles are from Wang et al. (2013) and Wu et al. (2014).

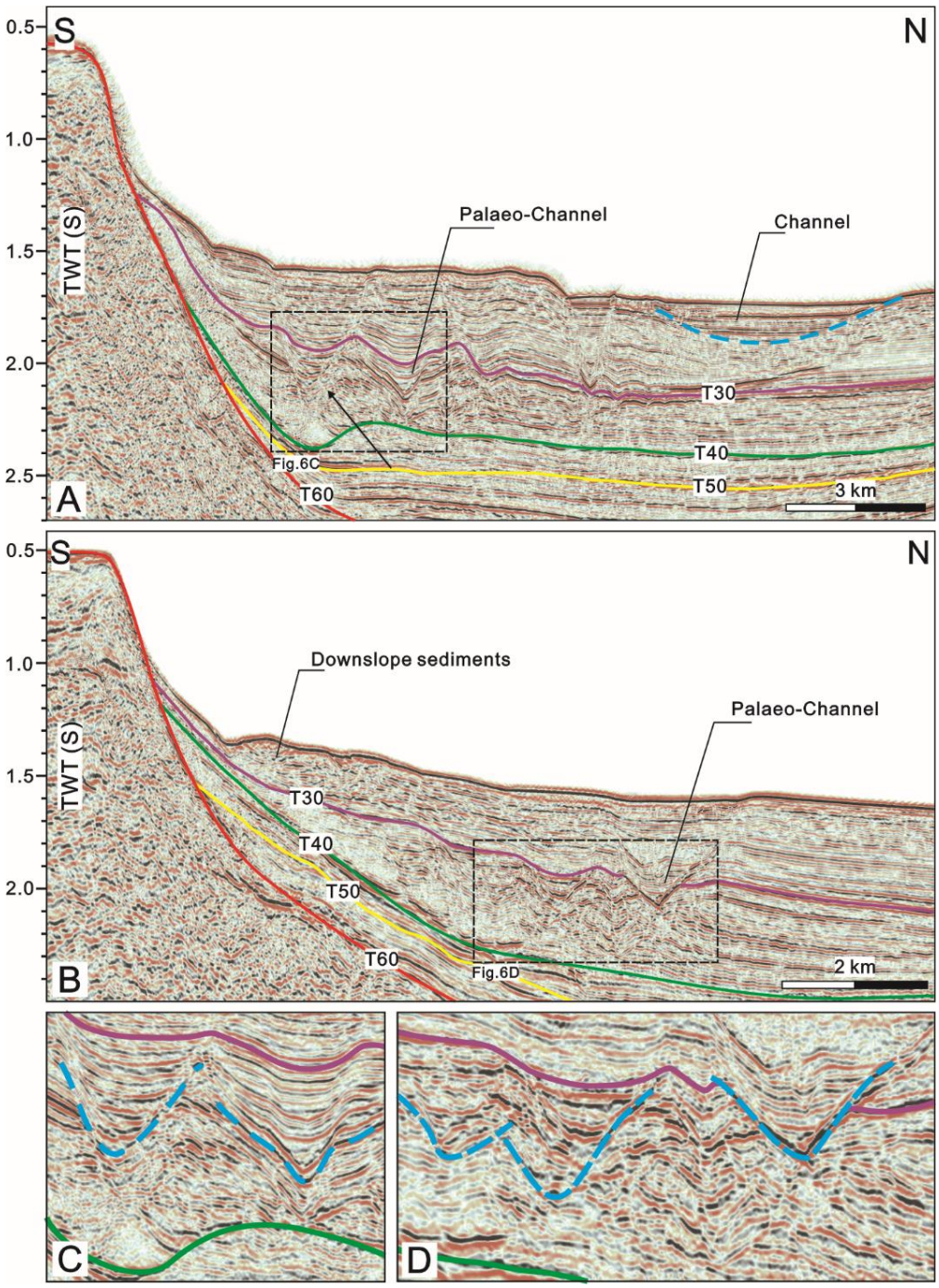

Fig.6 A) and B) Seismic profiles imaging the northeast flank of the ZCP. The blue dashed line indicates a buried channel close to the seafloor. The locations of seismic profiles are shown in Fig.1B. C) and D) Zoomed-in seismic profiles showing the palaeo-channels (shown as blue dashed lines) in strata beneath Horizon T30. Purple and green solid lines indicate Horizons T30 and T40, respectively. The interpretation is based on the original seismic data after Wang et al. (2013) and Wu et al. (2014).

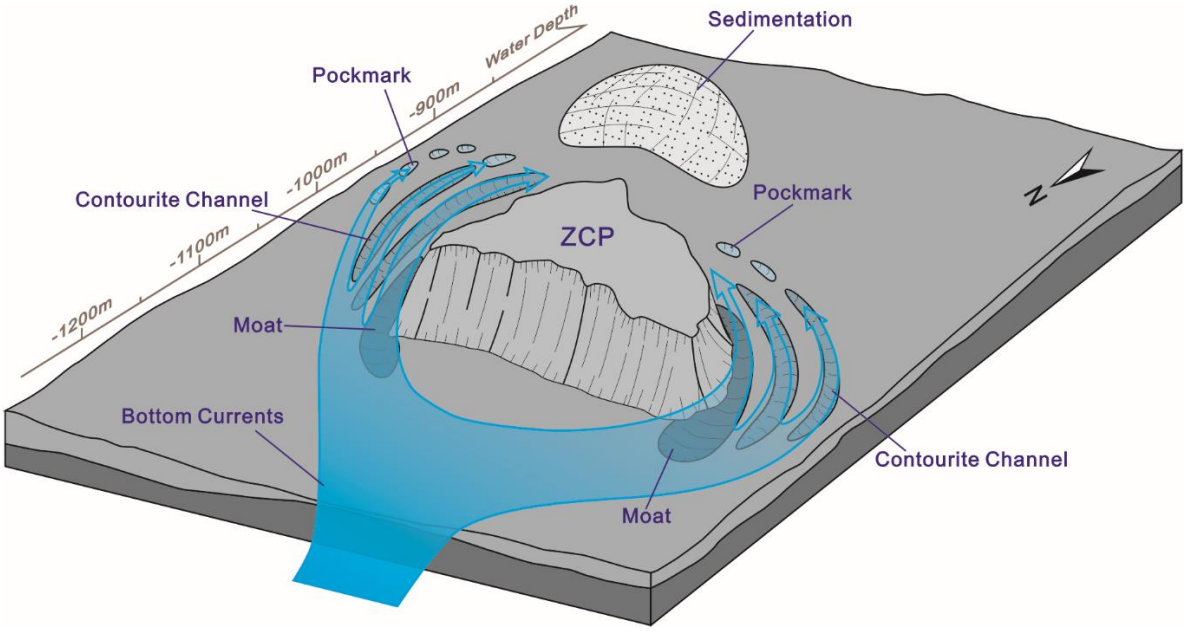

Fig.7 Sketch summarizing the pathways of bottom currents around the ZCP and how seafloor morphology influences the dynamics of bottom currents. In the study area, the bottom currents are proposed to flow from the north and to the south, and split by the obstacle of ZCP. The existence of obstacle has led to the enhancement of bottom current erosion on the south flanks of platform, especially close to the slope bottom of ZCP. Therefore, on the flanks of ZCP, the erosional moats were formed at the bottom of slopes and pockmark trails are involved into contourite channels under the bottom current erosion. Furthermore, due to the long-distance (tens of kilometres) upslope transportation (from north to south), the sediment transport capacity of bottom currents has significantly decreased. The suspending sediments carried by bottom currents hence deposited at the south region of ZCP, which is covered by a large area of smooth seafloor with rare erosional features.